Electrocatalytic hydrogenation of glucose and xylose using carbon fiber supported Au nanocatalysts

Oña, Jay Pee; Latonen, Rose Marie; Kumar, Narendra; Peurla, Markus; Angervo, Ilari; Grénman, Henrik

Published in:
Electrochimica Acta

DOI:
10.1016/j.electacta.2022.140754

Published: 10/09/2022

Document Version
Final published version

Document License
CC BY

Electrochimica Acta 426 (2022) 140754

Contents lists available at ScienceDirect

Electrochimica Acta

journal homepage: www.journals.elsevier.com/electrochimica-acta

Electrocatalytic hydrogenation of glucose and xylose using carbon fiber supported Au nanocatalysts

Jay Pee Oña [a], Rose-Marie Latonen [b], Narendra Kumar [a], Markus Peurla [c], Ilari Angervo [d], Henrik Grénman [a,*]

[a] Industrial Chemistry and Reaction Engineering, Johan Gadolin Process Chemistry Centre, Faculty of Science and Engineering, Åbo Akademi University, Henriksgatan 2, Turku FI-20500, Finland
[b] Laboratory of Molecular Science and Engineering, Johan Gadolin Process Chemistry Centre, Faculty of Science and Engineering, Åbo Akademi University, Henriksgatan 2, Turku FI-20500, Finland
[c] Institute of Biomedicin, University of Turku, Kiinamyllynkatu 10, Turku FI-20520, Finland
[d] Wihuri Physical Laboratory, Department of Physics and Astronomy, University of Turku, Turku FI-20014, Finland

ARTICLE INFO

Keywords:
Au nanocatalysts
Carbon fiber
Electrocatalytic
Hydrogenation
Xylose
Glucose

ABSTRACT

Recent evidences have shown catalyst structure sensitivity of electrocatalytic hydrogenation (ECH) of organic molecules in aqueous phase. In this study, ECH of glucose and xylose was investigated using gold nanoparticles (AuNPs) on activated carbon fiber (CF) support as catalyst. CF supported AuNPs catalysts (CF/AuNPs) were synthesized by deposition-precipitation method and were characterized by physicochemical (SEM, TEM, XRD, N_2 physisorption, ICP-OES) and electrochemical methods. Chemical or thermal pre-treatment of CF prior to Au deposition resulted in different AuNPs size distributions. The activity towards glucose or xylose ECH were observed to be dependent on the particle size of AuNPs and the applied potential. Compared to a polycrystalline Au catalyst, higher reaction rates for glucose and xylose ECH were observed for a CF/AuNPs catalyst with a higher surface area. This indicates that the activity of Au towards glucose and xylose ECH is dependent on the surface area and particle size, and particle size control can be achieved by simple chemical or thermal pre-treatment of the catalyst support.

1. Introduction

Catalytic conversion of biomass into fuels and value-added chemicals is a viable technology that can reduce our dependence on fossil fuels and mitigate global warming [1]. In order to generate energy-dense chemicals and fuels, biomass-derived feedstocks need to be catalytically hydrogenated to achieve a high H:C ratio [2]. Catalytic hydrogenation of carbohydrates is conventionally carried out in batch-type slurry reactors operating at temperatures ranging from 80 to 150 ^{o}C and 30-70 bar hydrogen pressure [3]. High-purity hydrogen is mainly sourced from steam reforming of fossil-based fuels [4]. During the past several decades, electrocatalytic hydrogenation (ECH) of chemicals has gained interest due to its advantages such as *in-situ* generation of reductive equivalents, operability towards aqueous feedstocks, and relatively milder reaction conditions compared to most catalytic routes [5,6]. The energy required to drive ECH can be provided by renewable energy sources (e.g. solar, wind) thereby making it a sustainable process that could serve as an alternative to the conventional catalytic hydrogenation. However, fundamental understanding of the catalytic properties of the metal catalysts towards ECH of various biomass-derived substrates is still lacking.

The mechanism for electrocatalytic hydrogenation is assumed to proceed through a reaction between chemisorbed hydrogen (MH) and an adsorbed sugar molecule (M-$C_xH_yO_z$) (Eq. (2)). The chemisorbed hydrogen is formed by the electroreduction of water on the metal cathode upon application of a certain potential Eq. (1) [7]:

$$H_2O + e^- + M \rightarrow MH + OH^- \qquad (\textit{Volmer reaction}) \tag{1}$$

$$M - C_xH_yO_z + 2MH \rightleftharpoons 3M + C_xH_{y+2}O_z \tag{2}$$

In competition with Eq. (2) are the electrochemical Eq. (3) and chemical Eq. (4) hydrogen generation which also occur on the cathode surface:

* Corresponding author.
E-mail address: Henrik.Grenman@abo.fi (H. Grénman).

https://doi.org/10.1016/j.electacta.2022.140754
Received 17 February 2022; Received in revised form 21 April 2022; Accepted 20 June 2022
Available online 21 June 2022

$$MH + H_2O + e^- \rightleftharpoons M + H_2 + OH^- \quad (Heyrovsky\ reaction) \tag{3}$$

$$2MH \rightleftharpoons 2M + H_2 \quad (Tafel\ reaction) \tag{4}$$

The concurrent hydrogen evolution reactions (HER) decreases the current to drive ECH reactions and hence the Faradaic efficiency (*FE*) towards sugar alcohol product formation. Some of the first electrocatalysts used for the ECH of organic compounds were bulk metals such as Pt, Raney Ni and Devarda Cu [8–12]. However, highly dispersed supported metal nanocatalysts have shown enhanced activity and Faradaic efficiency (*FE*) towards ECH of oxygenated substrates like phenol and benzaldehyde [13–20], lactic acid [21], and furfural [22]. In these studies, the rate of ECH was sensitive to the nature of the metal [16,17,19], the catalyst surface area [14,15], binding energies between the substrate and the metal catalyst [19], and the effects of the catalyst support [13]. Earlier studies on the ECH of carbohydrates involved non-precious metals such as Ni, Raney Ni [23,24] and metals with high overpotential for hydrogen evolution reaction (HER) such as Pb [25] and Zn(Hg) [26]. In the work by Kwon et al. [7], ECH of glucose was studied on a large number of transition metal electrodes. A group of metals with high selectivity towards sorbitol formation was identified which included late-transition metals (Fe, Co, Ni, Cu, Pd, Au, and Ag). Most studies on the ECH of sugars focused on the effect of the electrode, electrolyte composition, and reaction conditions [7,11,23,25–29]. However, less is known about the effects of the catalyst structure textural properties of the catalyst and cluster size of the metal catalyst on these reactions.

In this work, the electrocatalytic hydrogenation of glucose and xylose on activated carbon fiber-supported Au nanoparticles (AuNPs) was investigated. Glucose and xylose are two of the main components of wood hemicellulose [30], a potentially sustainable source of fuels and chemicals. Hemicellulose can be obtained from wood biomass through extraction using pressurized hot water or subcritical water [31–33]. Acid hydrolysis of wood hemicellulose in batch or continuous mode yields sugar monomer products for further processing [34–36]. Glucose and xylose can be hydrogenated into sorbitol and xylitol respectively, which are valuable compounds used in the industry as food additives and platform chemicals [37,38]. Gold was chosen as the metal catalyst in this study for both glucose and xylose ECH as it showed high selectivity and appreciable activity towards sorbitol formation as observed in the study conducted by Kwon et al. [7] for the ECH of glucose. The present study went further to use dispersed gold on carbon as catalyst to reveal the effect of the metal cluster size on the overall catalytic activity, which has not been reported for the ECH of sugars to the best of our knowledge. As observed, the method of pretreatment of the carbon fiber support influenced the resulting Au cluster size for catalysts prepared under identical conditions.

2. Experimental

2.1. Materials

Hydrogen tetrachloroaurate (III) ($HAuCl_4$) hydrate (49 % Au) was obtained from Alfa Aesar/ABCR GmbH. The D-glucose (BioUltra, ≥ 98% wt.) and D-xylose (BioUltra, ≥ 99% wt.) powder reagents were obtained from Sigma-Aldrich. NaOH (p.a. grade, 99 %) and ammonium hydroxide (NH_4OH) solution (32 % wt.) were obtained from Merck. Activated carbon fiber (CF) (0.60 mm thickness) was purchased from Kynol®. All other chemicals were of reagent grade. Deionized water (resistivity 18 MΩ·cm) was used to prepare all solutions.

2.2. Fabrication of CF/AuNPs catalysts

Carbon fiber was modified with gold nanoparticles (AuNPs) via a deposition-precipitation method developed by Behravesh et al. [39]. Deposition-precipitation method was used to synthesize the catalysts in this study to evaluate the effect of pre-treatment of the catalyst support (carbon fibers) on the resulting AuNPs size and Au dispersion. Hydrogen tetrachloroaurate (III) ($HAuCl_4$) hydrate was used as gold precursor and ammonium hydroxide (NH_4OH) as precipitating agent. Prior to modification, the CF support was subjected to chemical or thermal pre-treatment. The chemical pre-treatment involved immersing the CF in acid (0.5 M HCl) or base (0.5 M NaOH) for 3 h with gentle stirring. The chemically treated CF was then washed with 2000 mL distilled water and dried at 100 °C for approximately 12 hours. The thermal pre-treatment involved calcination of the CF support at 225 °C or 325 °C using a step calcination procedure. The pre-treated and untreated (pristine) CF supports were immersed in a 0.4 g/L solution of the gold precursor. The pH was adjusted to 10.5 by adding 32 % wt. ammonium hydroxide solution (NH_4OH) while the mixture was vigorously stirred. The mixture was stirred overnight at room temperature. The CF/AuNPs catalysts were rinsed with excess H_2O and dried at 100 °C for 6 h. The catalysts were then calcined at 300 °C in a muffle oven in the presence of air using a step calcination procedure in order to eliminate the residual chloride ions from the catalysts.

2.3. CF and CF/AuNPs characterization

The physicochemical characterization of the CF and CF/AuNPs materials were carried out using nitrogen physisorption, Transmission Electron Microscopy (TEM), Inductively Coupled Plasma Optical Emission Spectroscopy (ICP-OES), Scanning Electron Microscopy/Energy Dispersive X-ray Analysis (SEM/EDXA), and X-ray Diffraction (XRD). The electrochemical characterization of the CF and CF/AuNPs was carried out using linear sweep voltammetry (LSV).

The specific surface area and the pore volume of the catalysts were measured using nitrogen physisorption. The instrument used was MicroActive 3FlexTM 3500 (Micromeritics). Before the analysis, the catalysts were outgassed for 4 h at 150 °C. The Dubinin-Radushkevich equation was used to calculate the surface area, whereas the Horvath and Kawasaki method was used to calculate the micropore volume of the pristine and pretreated CF, as well as the CF/AuNPs catalysts [40].

The surface morphology of the synthesized CF/AuNPs catalysts such as crystal shape, size and distribution was analysed via SEM/EDXA using a Leo Gemini 1530 scanning electron microscope with a Thermo Scientific UltraDry Silicon Drift Detector. Transmission electron microphotographs of the catalysts were obtained using a JEOL JEM 1400 Plus transmission electron microscope operated at 120 kV acceleration voltage and 0.38 nm resolution. ImageJ was used for calculating the AuNPs average particle sizes and distributions, and a sample size of 600-800 particles was used for each catalyst. The gold content of the fabricated CF/AuNPs catalysts were analysed by ICP-OES (Varian Liberty 110 ICP Emission Spectrometer) using argon plasma to excite the Au atoms for the measurement of optical emission. Before the ICP-OES analysis, a sample size of 0.10-0.14 g was dissolved in 50 mL concentrated H_2SO_4 and digested at 150 °C using a microwave heater and thereafter diluted to 100 mL.

The structural and phase properties of the CF/AuNPs catalysts were determined using X-ray powder diffractometer (PANalytical Empyrean) with five axis goniometer. The X-ray tube used was Empyrean Cu LFF and the X-ray radiation was filtered to include only Cu $K_{\alpha1}$ and Cu $K_{\alpha2}$ components. The results were analysed using MAUD (Material Analysis Using Diffraction) analysis program.

Linear sweep voltammetry was carried out using a single-compartment, three-electrode electrochemical cell connected to the Autolab (PGSTAT20) General Purpose Electrochemical System at room temperature (23 ± 1 °C). The CF or CF/AuNPs working electrode (WE) was constructed by attaching the CF or the fabricated CF/AuNPs on a glassy carbon (GC) disk electrode using carbon glue (Electrodag® PF-407C). The glue was allowed to dry overnight. The resulting WEs had a geometric area of 0.07 cm^2. The polycrystalline Au electrode was prepared by mechanical polishing using 0.3 μm alumina followed by

rinsing with water and sonication. The geometric area of the polycrystalline Au electrode was 4 cm^2. The counter electrode (CE) used was a glassy carbon rod and the reference electrode was Ag/AgCl/3M KCl (Thermo Scientific Orion™ 900100). All the potentials were measured against this Ag/AgCl/3M KCl reference electrode. Glucose or xylose was dissolved into the supporting electrolyte solution (0.1 M Na_2SO_4) to make a concentration of 0.1 M. The electrolyte solution with or without sugar was initially purged with N_2 for 15 min and the N_2 gas was kept above the solution during the LSV experiments. All current densities reported were calculated using the geometric area of the working electrodes.

The electrochemically active surface areas (ECSA) of the CF/AuNPs catalysts were estimated from the charge of gold oxide reduction using the procedure described by Trasatti and Petrii [41]. The CV measurements were carried out in the H-shaped electrochemical cell (Latech) set up. ECSA was calculated from the reference charge of 390 μC cm^{-2}, which corresponds to the charge required to reduce one monolayer of AuO per unit area. The activities of the CF/AuNPs catalysts toward glucose and xylose ECH were normalized with the calculated ECSA.

2.4. Electrocatalytic hydrogenation of glucose and xylose

The constant-potential electrolysis experiments were conducted to quantify the products and determine the Faradaic efficiency (*FE*) towards sorbitol and xylitol production. For these experiments, a three-electrode set-up was employed using an H-shaped electrochemical cell (Latech) divided by a Nafion 117 membrane (Ion Power, Inc.) as shown in Fig. 1. Prior to use, the electrochemical cell and other glassware were cleaned by immersing them in a 1:1 mixture of sulfuric and nitric acid overnight followed by boiling in ultrapure water (resistivity 18 MΩ·cm). Pretreatment of the Nafion membrane involved boiling in H_2O_2 solution (3 % vol.) for 1 h and in sulfuric acid (2 M) for 1 h, with rinsing in deionized water in between and after the boiling steps. The working electrode was a CF/AuNPs glued onto a carbon rod (99.999% carbon, Strem Chemicals Inc.) or a polycrystalline Au electrode. The geometric area of the working electrode was 2 cm^2 for the CF/AuNPs catalyst and 4 cm^2 for polycrystalline Au. The conductive carbon rod was used as the counter electrode to avoid metal contamination of the electrolysis set-up. The working and reference electrodes were immersed in the cathodic compartment containing 25 mL of 0.1 M Na_2SO_4 with 0.1 M glucose or xylose. The counter electrode was placed in the anodic compartment containing 25 mL of the supporting electrolyte solution (0.1 M Na_2SO_4). The designated potential was applied on the working electrode by the Autolab (PGSTAT20) potentiostat for a certain duration, after which the sample solution was collected and analysed. The hydrogenation rate was expressed as mmol of sorbitol or xylitol produced per hour. During the electrolysis, mass transport of the sugar monomer was facilitated using a magnetic stirrer at approximately 500 rpm.

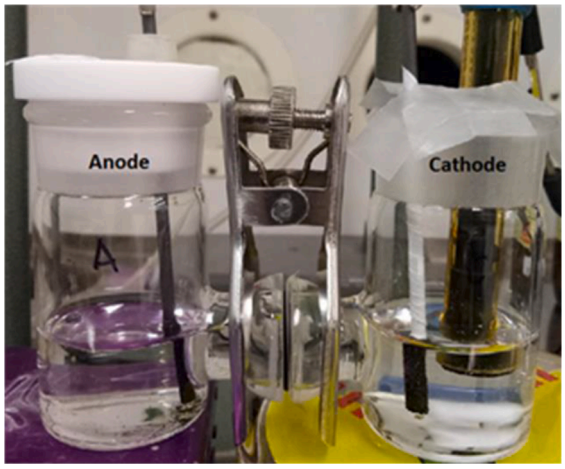

Fig. 1. Experimental set-up for constant-potential electrolysis.

2.5. Product analysis

Samples collected from the cathodic compartment after electrolysis were pretreated and analysed using HPLC equipped with a refractive index detector. The HPLC column used for analysis could not tolerate high concentrations of salt, and therefore pretreatment of the HPLC samples by extraction of salt ions was necessary. Pretreatment of the samples involved passing 1 mL sample volume into strong anion and cation exchange SPE tubes (Supel™, Merck) to remove the ions of the supporting electrolyte. The HPLC column (Aminex HPX-87C) was maintained at 80 °C and the eluent used was 1.2 mM CaSO4 solution. Calibration curves were constructed with sorbitol and xylitol standard solutions by plotting the peak areas versus the sugar alcohol concentrations. The *FE* towards the formation of the sugar alcohol product (sorbitol or xylitol) measured by HPLC was calculated using the following equation:

$$FE\ (\%) = \frac{\text{mol of sorbitol or xylitol formed}}{\text{total charge passed (C)} \ / \ (\text{F} * 2)} \text{ x } 100\% \quad (5)$$

Where the total charge is expressed in coulombs (C) and *F* is the Faraday's constant (96,485 C mol^{-1}).

3. Results and discussion

3.1. Characterization of CFs and CF/AuNPs materials

3.1.1. Physical and electrochemical surface area

The surface properties of pristine and treated carbon fiber (CF) were studied using SEM and N_2 physisorption. Table S1 shows the specific surface areas and pore volumes of pristine CF (CF-1), HCl-treated CF (CF-2), NaOH-treated CF (CF-3), CF calcined at 225 °C (CF-4), and CF calcined at 325 °C (CF-5). An increase in surface area and pore volume of the pristine CF after chemical treatment with HCl or NaOH was observed. A plausible explanation for this is the surface modification of the carbon fibers resulting from the HCl and NaOH treatments giving rise to variations in pore dimensions. It is also noteworthy to mention that thermally pretreated carbon fibers at 225 °C and 325 °C showed a decrease in the surface area and pore volume compared to pristine CF. This decrease in the surface area and pore volume can be attributed to distortion of the structural features of the carbon fibers, which can be observed in the SEM micrographs of the thermally treated CFs (Figure S1d-e).

SEM images of the pristine carbon fiber and AuNPs-modified CF following various pretreatments are shown in Fig. 2. It is evident that the deposition of AuNPs and subsequent calcination influenced the surface characteristics of the catalysts (Fig. 2b-f) compared to the pristine CF (Fig. 2a). In all the prepared CF catalyst supports, Au particles were deposited both on the surface and inside the pores of the support. After gold deposition, there was a general decrease in the surface area and pore volume with all types of CF supports. This is attributed to the deposition of Au nanoparticles into the pores of the support and blocking of the pores with Au nanoparticles. Compared to CF-1/AuNPs, CF-2/AuNPs and CF-3/AuNPs obtained higher actual Au loading (shown in Table 1). SEM images confirm that AuNPs were deposited on the CF surface and also within the pores in CF-2/AuNPs (Fig. 2c) and CF-3/AuNPs (Fig. 2b) at a higher degree than in CF-1/AuNPs (Fig. 2b). This explains the lower surface area of CF-2/AuNPs and CF-3/AuNPs compared to CF-1/AuNPs, as the "unoccupied" pores in CF-1/AuNPs contribute to a higher specific surface area (Table 1). Lower surface areas were obtained for CF-4/AuNPs and CF-5/AuNPs than the other catalysts mainly due to the lower surface area of the thermally treated CF supports.

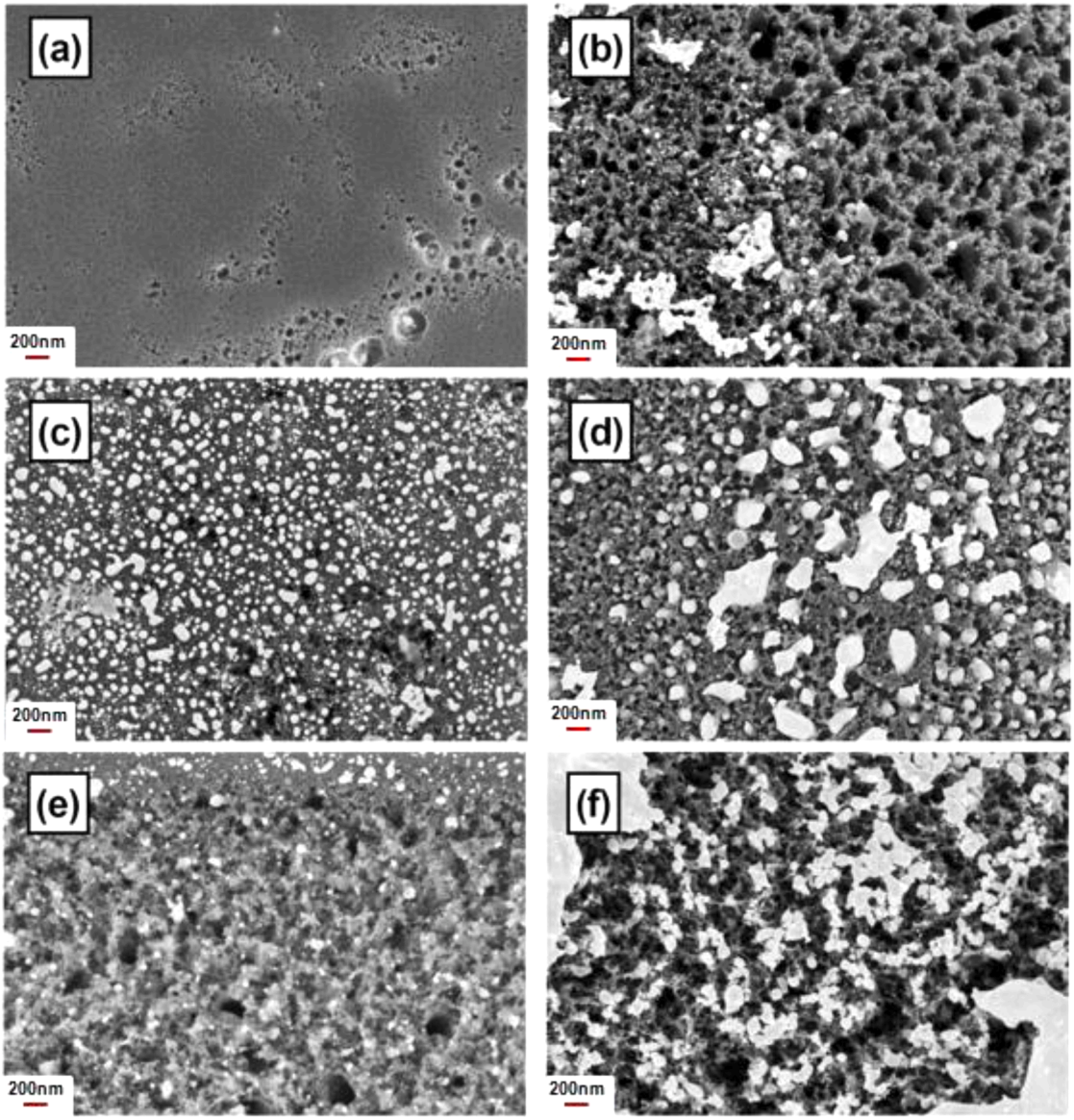

Fig. 2. Scanning electron micrographs of pristine CF (a), and CF/AuNPs with: untreated CF (CF-1/AuNPs) (b), HCl-treated CF (CF-2/AuNPs) (c), NaOH-treated CF (CF-3/AuNPs) (d), CF calcined at 225 °C (CF-4/AuNPs) (e), CF calcined at 325 °C (CF-5/AuNPs) (f).

Table 1
Physico-chemical characterization data of the catalysts: Au loading, Au average cluster size, specific surface area and pore volume.

Sample	Nominal Au loading (wt %)	Measured Au loading (wt %)	Loading efficiency (%)	Au average size (nm)	Au dispersion (%)	Specific surface area (m^2/g)	Pore volume (cm^3/g)
CF-1/ AuNPs	2.0	0.19 ± 0.01	10	10.2 ± 8.6	11.7	1887	0.69
CF-2/ AuNPs	2.0	0.90 ± 0.01	45	19.9 ± 15.8	5.8	1765	0.65
CF-3/ AuNPs	2.0	1.27 ± 0.03	65	7.6 ± 6.1	14.6	1772	0.64
CF-4/ AuNPs	2.0	0.83 ± 0.05	40	18.9 ± 11.8	6.2	1634	0.66
CF-5/ AuNPs	2.0	1.62 ± 0.03	80	20.6 ± 15.3	5.8	1651	0.66

Independent of the type of CF pretreatment, Au particles were deposited both as dispersed nanoparticles and as large aggregates. The formation of large particles is due to the interaction of the precursor ($HAuCl_4$) with carbon which results in metal reduction [42].

$$4\ C + [Aucl_4]^- \rightarrow Au^0\ /\ C + 3\ Cl^-\ /\ C^+ + Cl^- \quad (6)$$

The above reaction (Eq. (6)) results in rapid adsorption of the metal on the external carbon surface. During the catalyst preparation, the CF support became glittery when it was soaked in the $HAuCl_4$ solution. This

was also observed in earlier works where Au/activated carbon catalysts were prepared from $HAuCl_4$ using deposition-precipitation method [43, 44]. Therefore, the choice of pretreatment of carbon fiber, method used for preparation of AuNPs, activation procedure and type of Au precursor can have a direct effect on the physico-chemical properties of the CF/AuNPs catalyst produced.

In terms of the electrochemical surface area (ECSA), the values obtained (Table S2) relate primarily to the actual gold content in the CF/AuNPs catalysts. This would explain, for instance, the higher ECSA of CF-3/AuNPs than CF-1/AuNPs despite the higher physical area of the latter. However, the method used for ECSA calculation also include significant contribution from capacitive currents especially for microporous materials like CF, which makes interpretation of results more difficult.

3.1.2. *Au particle size distributions and Au dispersions of the different CF/AuNPs catalysts*

The Au content of the fabricated CF/AuNPs catalysts was measured using ICP-OES and the loading efficiency on the CF support was determined from the actual Au content. Using the deposition-precipitation

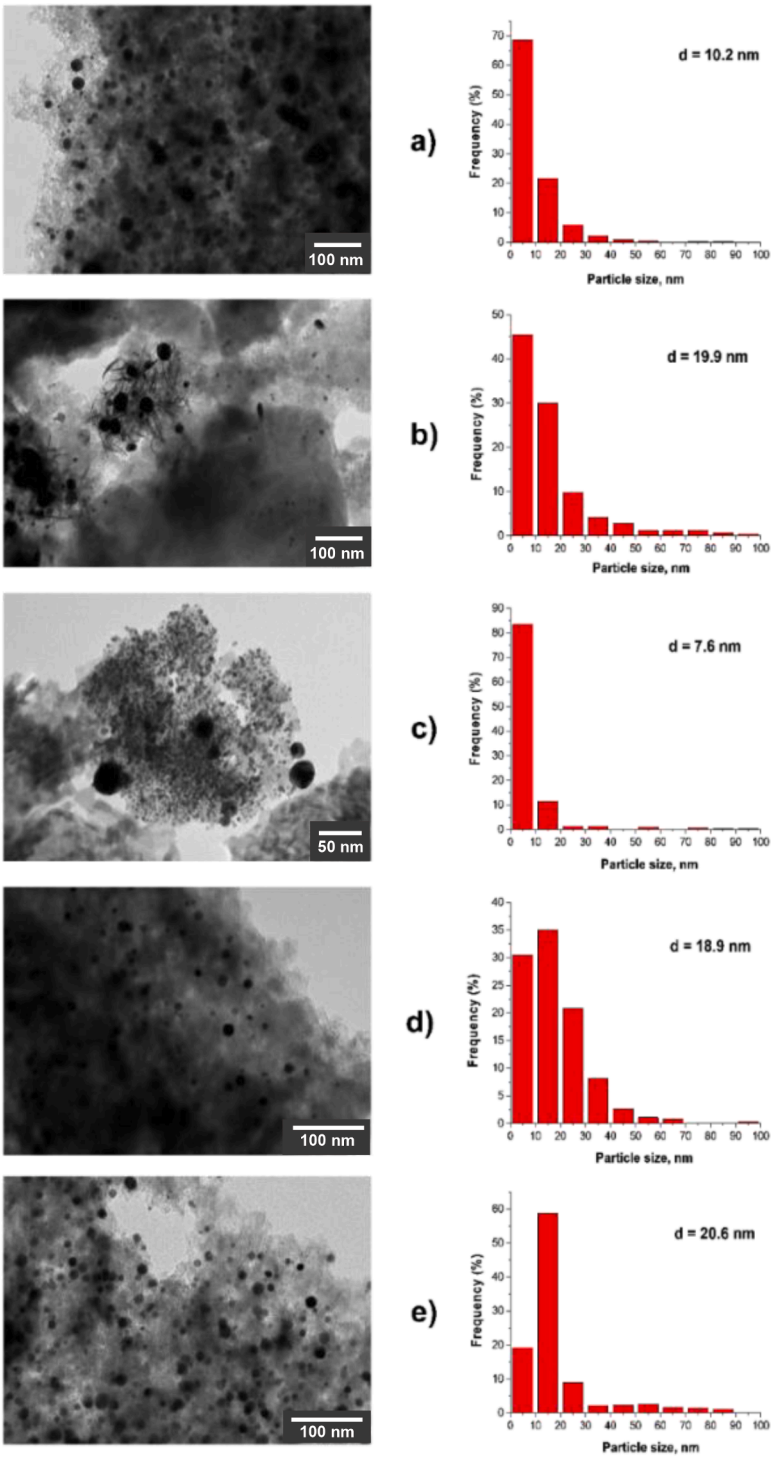

Fig. 3. TEM images and particle size distributions of CF-1/AuNPs (a), CF-2/AuNPs (b), CF-3/AuNPs (c), CF-4/AuNPs (d), and CF-5/AuNPs (e).

method, AuNPs loading efficiency of 10-80 % was achieved, which varied among the different types of CF support prepared (Table 1).

The Au nanoparticles size measurements were carried out by TEM. The images and particle size distributions of all the fabricated CF/AuNPs catalysts are illustrated in Fig. 3 and the average Au cluster sizes are listed in Table 1. CF-1/AuNPs with untreated CF had an average Au cluster size of 10.2 nm. NaOH-treatment of the CF support resulted in the smallest Au clusters with an average size of 7.6 nm (CF-3/AuNPs). The largest average Au cluster size was observed for the CF/AuNPs catalysts with CF calcined at 325 ^{o}C (CF-5/AuNPs – Fig. 3e) with an average Au cluster size of 20.6 nm. The CF/AuNPs catalysts with CF pretreated with HCl (CF-2/AuNPs - Fig. 3b) and CF calcined at 225 ^{o}C (CF-4/AuNPs - Fig. 3d) had comparable average Au cluster sizes of 19.9 nm and 18.9 nm, respectively. Hence, it can be concluded that pretreatment of CF support influenced the distribution and size of AuNPs. Diffraction data show high intensity peaks close to 38.1^{o}, 44.3^{o}, 64.5^{o}, 77.5^{o}, 81.7^{o}, 98.2^{o}, 110.8^{o}, and 115.2^{o} for all types of CF/AuNPs catalysts (Figure S3). These details can be explained with the Au phase. The crystal model for Au which is being used, and which matches well with diffraction data, corresponds to the face centered cubic crystal structure with space group (Fm-3m). The highest peak intensities were observed with CF-2/AuNPs. On the other hand, differences in peak intensities were negligible between CF-4/AuNPs and CF-5/AuNPs as well as between CF-1/AuNPs and CF-3/AuNPs.

The Au dispersion (D_{Au}) refers to the ratio of surface atoms to the total number of atoms and can be estimated from the Au cluster diameter (d) using the following equation [39]:

$$D_{Au} = \frac{6M}{d\rho a_{Au} N_A} * 100\% \quad (7)$$

where M is the molar mass of gold (0.197 kg/mol), ρ is the density of Au (1.932 x 10^4 kg/m^3), a_{Au} is the effective surface area of one Au atom (8.7 x 10^{-20} m^2), and N_A is the Avogadro number. Eq. (7) shows an inverse relationship between dispersion and the Au cluster size. Taking the average Au cluster size obtained from TEM analysis, Table 1 shows the Au dispersions of the CF/AuNPs catalysts. From TEM, CF-3/AuNPs showed the smallest Au particle size (7.6 nm) and therefore had the highest Au dispersion.

3.1.3. Linear sweep voltammetry

Fig. 4 shows the linear sweep voltammograms of the polycrystalline Au and a CF (non-treated)/AuNPs electrodes in sugar-free "blank" solution (dashed lines in both Figs. 4a and 4b) and in 0.1 M glucose (Fig. 4a, solid lines) and 0.1 M xylose (Fig. 4b, solid lines). The cathodic currents generated in the blank experiments are attributed to the evolution of H_2.

On a polycrystalline Au electrode, the cathodic currents produced in the presence of glucose were lower than those generated in the blank solution (Fig. 4a, solid red line). This suggests that the presence of glucose inhibits hydrogen evolution, possibly due to adsorption of glucose molecules on the electrode surface. On the other hand, in the xylose solution, the cathodic currents generated starting from ca. -1.1 V were larger than those recorded in the blank solution (Fig. 4b, solid red line). The higher cathodic current produced in the presence of xylose may be attributed to the electrohydrogenation of xylose in addition to H_2 evolution.

The cathodic currents produced on the CF/AuNPs electrode (Fig. 4, solid blue and solid green lines) in the presence of either glucose or xylose were higher than in the blank experiment suggesting that sugar hydrogenation occurs concurrently with H_2 evolution. However, at more negative potentials (starting from ca. -1.4 V in glucose solution and ca. -1.7 V in xylose solution), cathodic currents were higher in the blank experiment which indicates HER inhibition in the presence of the sugar.

The linear sweep voltammograms of all the CF/AuNPs catalysts show an increase in cathodic current starting from ca. -1.2 V both in the presence of sugars (Fig. 5a-b, insets) and in the background electrolyte (Figure S4). Towards more negative potentials, the cathodic currents recorded for CF-5/AuNPs, with CF calcined at 325 ^{o}C, were lower than for the other CF/AuNPs catalysts. This is mainly due to the lower ECSA of CF-5/AuNPs compared to the other CF/AuNPs catalysts.

3.2. Electrocatalytic hydrogenation of sugars on polycrystalline Au and CF/AuNPs catalysts

3.2.1. Comparison of activities and FEs between polycrystalline Au and CF/AuNPs catalyst

To observe the effect of using a nanostructured Au catalyst, the activity and faradaic efficiency of a CF (non-treated)/AuNPs catalysts were compared to a polycrystalline Au catalyst. The activities and conversion

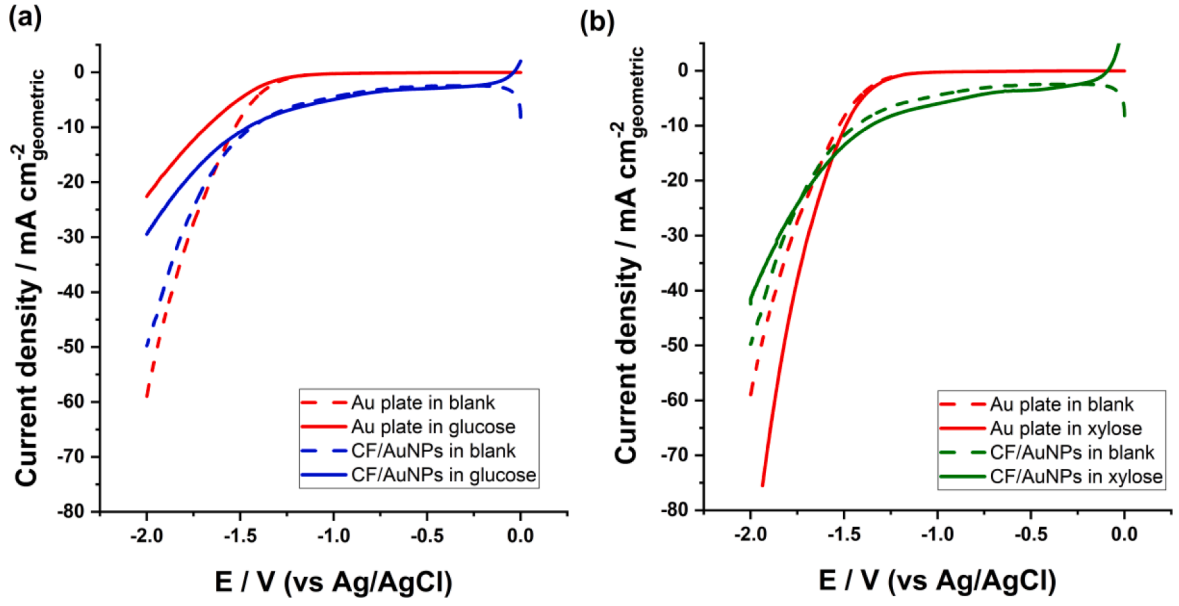

Fig. 4. Linear sweep voltammograms of polycrystalline Au and GC/CF/AuNPs electrodes in 0.1 M Na_2SO_4 without (dashed lines) and with (solid lines) 0.1 M glucose (a) and 0.1 M xylose (b). The scan rate is 1 mV/s.

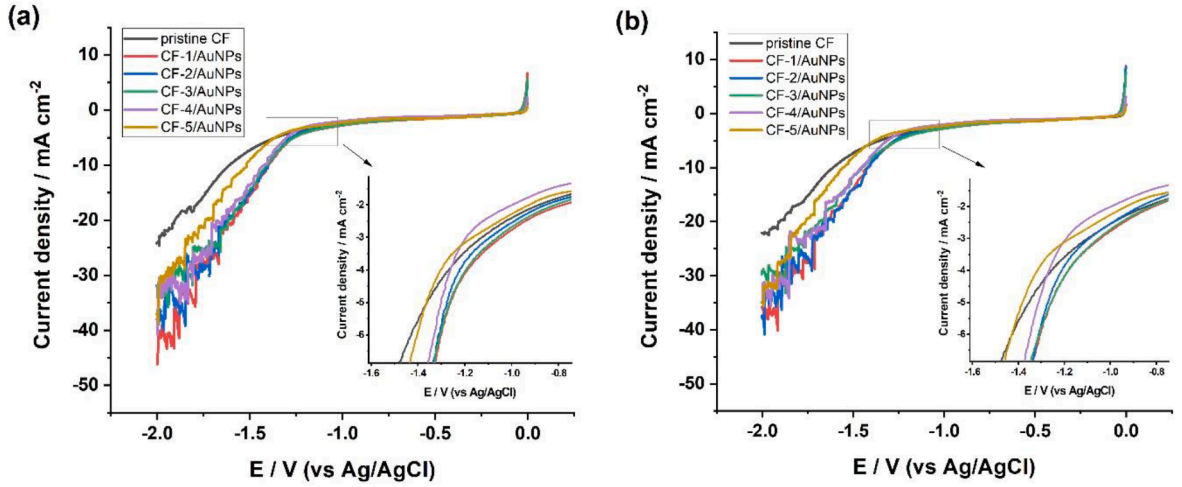

Fig. 5. Linear sweep voltammograms of GC/CF and GC/CF/AuNPs electrodes with different CF pretreatments in 0.1 M glucose (a) and 0.1 M xylose (b) solutions. The scan rate is 1 mV/s. The current density is calculated based on the geometric area. Insets in both figure show a magnified portion of the voltammogram where cathodic currents start to increase.

efficiencies towards sugar hydrogenation of the polycrystalline Au and CF/AuNPs catalysts were tested by performing ECH of glucose and xylose at various applied potentials in the H-cell described in Section 2.4. Catalytic activity was expressed as the amount of sorbitol or xylitol produced per hour and was not normalized to ECSA as the capacitive currents in CF/AuNPs contribute significantly to ECSA determination (please see discussion in Section 3 of supporting information).

Fig. 6 shows the rate of sorbitol and xylitol formation (blue and green bars, respectively) for the tested catalysts at each applied potential and the corresponding Faradaic efficiencies (connected red points). On the polycrystalline Au catalyst, the highest rate of sorbitol formation (0.005 mmol/h) was observed at -1.4 V (Fig. 6a) while the highest rate of xylitol formation (0.014 mmol/h) was observed at -1.6 V (Fig. 6c). These optimum potentials were comparable to that obtained by Kwon et al. [7] (-1.05 V vs RHE, pH = 7) for the ECH of glucose over polycrystalline Au electrode. Furthermore, the rate of xylitol formation was also higher than that of sorbitol at any applied potential, suggesting that the reactivity of xylose towards ECH is higher than that of glucose. The *FE* (connected red dots) for both sorbitol (4.4 % - Fig. 6a) and xylitol (6.1 % - Fig. 6c) formation reached a maximum at -1.3 V, beyond which the

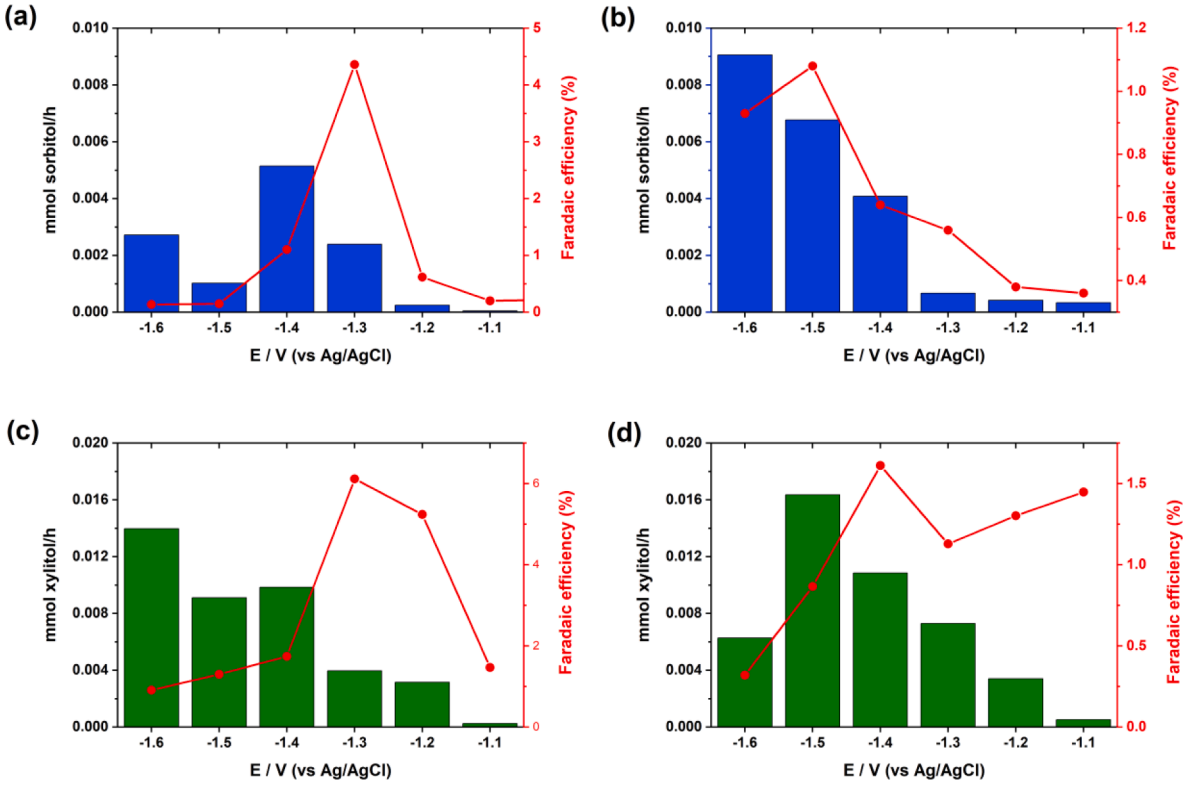

Fig. 6. Hydrogenation rates (mmol sorbitol/h-blue columns, or mmol xylitol/h-green columns) and FE (connected red dots) at various applied potentials of glucose ECH on polycrystalline Au (a) and CF(non-treated)/AuNPs (b); and xylose ECH on polycrystalline Au (c) and CF(non-treated)/AuNPs (d). Reaction conditions: 0.1 M of glucose or xylose in 0.1 M Na_2SO_4 supporting electrolyte, stirring speed of 500 rpm, ambient temperature and pressure, constant flow of N_2 above the reaction solution.

supplied potential goes mainly towards H_2 evolution.

On the CF/AuNPs catalyst, the highest rate of sorbitol formation (0.009 mmol/h) was observed at -1.6 V (Fig. 6b) while that for xylitol (0.016 mmol/h) was observed at -1.5 V (Fig. 6d). The rate of formation of sorbitol and xylitol on the CF/AuNPs catalyst generally increased as the applied potentials became more negative. The rate for xylitol formation however, decreased at -1.6 V (0.006 mmol/h – Fig. 6d) after reaching a maximum at -1.5 V. The *FE* towards sorbitol formation also gradually increased as the applied potentials became more negative and reached a maximum at -1.5 V (1.1 % - Fig. 5b). The *FE* for xylitol formation on the other hand showed a maximum at -1.4 V (1.6 % - Fig. 6d). The decrease in *FE* in both reactions is mainly attributed to the dominance of the H_2 evolution reaction.

The rates of sorbitol or xylitol formation as a function of applied potentials were generally higher for the CF/AuNPs catalyst than polycrystalline Au. This difference may be related to the number or type of active sites present in these catalysts, as well as their surface areas. Comparison of activity between CF/AuNPs and polycrystalline Au in terms of the ECSA may not be valid due to the limitations of the method used for ECSA determination when applied to CF/AuNPs. However, ECH rates normalized to geometric areas show higher activity of the CF/AuNPs catalyst than polycrystalline Au (Table S4). This highlights the advantage of using dispersed metal nanocatalysts as previously observed in the ECH of other organic compounds [13–15,21,22]. The Faradaic efficiencies however, were relatively lower for the CF/AuNPs catalyst than polycrystalline Au. This indicates that the kinetics for molecular hydrogen formation from chemisorbed hydrogen (Eq. (4)) is faster on the CF/AuNPs catalyst than on polycrystalline Au.

Based on literature, higher yields and selectivities for sugar ECH were obtained using nonprecious metal and metal alloys such as Raney Ni, Pb, and Zn(Hg) [7,11,23]. Park et al. reported a 79 % FE towards sorbitol formation for the ECH of glucose in an undivided packed-bed flow reactor with $CaBr_2$ as supporting electrolyte [23]. Lessard et al. obtained moderate sorbitol FEs from 40 to 47% for the ECH of glucose over Raney Ni in both batch and flow reactor configurations [11]. Pb [7] and Zn(Hg) [23] were also active towards glucose ECH, although at higher applied potentials than Raney Ni. Although the FEs obtained for polycrystalline Au and CF/AuNPs in this work were significantly lower, the present study demonstrates that reaction rates for sugar ECH can be improved by using nano-sized Au catalyst, a less hazardous alternative to Raney Ni, Pb, or Zn(Hg). The catalytic activity and FE were observed to be sensitive to the Au cluster size in the different types of CF/AuNPs studied.

3.2.2. *Electrocatalytic activity of the different types of CF/AuNPs catalysts*

The electrocatalytic activities toward glucose and xylose ECH of the different types of CF/AuNPs catalysts prepared were tested using constant-potential electrolysis experiments. The catalytic activities of the CF/AuNPs catalysts were normalized with respect to their ECSA (see Table S2 in Supporting Information). Analysis of variance (one-way ANOVA) of the ECSA-normalized sorbitol and xylitol yields among the various CF/AuNPs catalysts show significant differences at 95% confidence level (see Section 6 of supporting information).

Table 2 shows the electrolysis data for glucose ECH over the different types of CF/AuNPs catalysts. The highest average current density (based on geometric area) during prolonged electrolysis was recorded for the CF-3/AuNPS catalyst (15.7 mA/cm^2) which had an NaOH-treated CF support. CF-1/AuNPs with a non-treated CF support had a comparable current density (15.6 mA/cm^2) but with a lower *FE* (0.2 %) than CF-3/AuNPS (0.3 %). CF-4/AuNPs (with CF calcined at 225 ^oC) and CF-5/AuNPs (with CF calcined at 325 ^oC) also had comparable current densities (7.4 and 6.6 mA/cm^2, respectively). However, CF-4/AuNPs had 4 times higher *FE* (0.4 %) than CF-5/AuNPs (0.1 %). CF-2/AuNPs, with an HCl-treated CF support, had a higher current density (9.8 mA/cm^2) than CF-4/AuNPs but with a comparable *FE* (0.4 %). Based on the ECSA-normalized sorbitol yields, CF-4/AuNPs had the highest specific activity (0.24 μM sorbitol/cm$^2_{ECSA}$) and highest *FE* (0.4 %) among the different CF/AuNPs catalysts studied. Although the highest sorbitol yield was obtained for the CF-3/AuNPs catalyst, its specific activity (0.10 μM sorbitol/cm$^2_{ECSA}$) was 2 times lower than CF-4/AuNPs owing to its high ECSA. This indicates that the surface active sites are more efficiently utilized for glucose ECH in CF-4/AuNPs than in CF-3/AuNPs as also reflected in the higher *FE* for CF-4/AuNPs. The catalytic activites towards glucose hydrogenation of the CF/AuNPs catalysts are associated to the presence of the metal (AuNPs), as negligible amounts of sorbitol were formed when glucose ECH was carried out using only the CF (non-treated) support as catalyst at the same reaction conditions. This observation further confirms the important role of AuNPs in the glucose electro-catalytic hydrogenations.

Table 2
Results obtained from the electrocatalytic hydrogenation of glucose using different types of CF/AuNPs electrode[a]

Working electrode	Average current density (mA/cm$^2_{geometric}$)	Total charge passed (C)	Sorbitol production (μM/cm$^2_{ECSA}$)	*FE* for sorbitol formation (%)
CF-1/AuNPs	15.6	667	0.16 ± 0.03	0.20 ± 0.07
CF-2/AuNPs	9.8	420	0.11 ± 0.02	0.40 ± 0.09
CF-3/AuNPs	15.7	673	0.10 ± 0.02	0.30 ± 0.07
CF-4/AuNPs	7.4	317	0.24 ± 0.05	0.40 ± 0.08
CF-5/AuNPs	6.6	280	0.12 ± 0.03	0.10 ± 0.05

[a] Reaction conditions: -1.5 V vs Ag/AgCl in 0.1 M Na_2SO_4 containing 0.1 M glucose for 6 h duration at room temperature and pressure. The values reflected are the average from three measurements.

The activities and *FE*s of the prepared CF/AuNPs catalysts toward xylose ECH were analyzed at the same applied electric potential (-1.5 V vs Ag/AgCl). The results are summarized in Table 3. Comparable current densities were recorded for CF-1/AuNPs (16.6 mA/cm^2) and CF-3/AuNPs (16.8 mA/cm^2). However, the specific activity for CF-3/AuNPs (0.34 μM xylitol/cm$^2_{ECSA}$) is 2 times lower than for CF-1/AuNPs (0.69 μM xylitol/cm$^2_{ECSA}$) owing to its higher ECSA. CF-2/AuNPs had a lower current density (10.6 mA/cm^2) than CF-3/AuNPs but had a higher specific activity (0.39 μM xylitol/cm$^2_{ECSA}$) and *FE* (1.2 %). This suggests higher surface utilization for xylose ECH in CF-2/AuNPs than in CF-3/AuNPs. Current densities were relatively lower for CF-4/AuNPs (8.2 mA/cm^2) and CF-5/AuNPs (5.8 mA/cm^2). However, due to their lower ECSAs, their specific activities toward xylose ECH were higher than for the other CF/AuNPs catalysts, 0.74 μM xylitol/cm$^2_{ECSA}$ for CF-4/AuNPs and 0.80 μM xylitol/cm$^2_{ECSA}$ for CF-5/AuNPs. The *FE*s of CF-4/AuNPs

Table 3
Results obtained from the electrocatalytic hydrogenation of xylose using different types of CF/AuNPs electrode[a]

Working electrode	Average current density (mA/cm$^2_{geometric}$)	Total charge passed (C)	Xylitol production (μM/cm$^2_{ECSA}$)	*FE* for xylitol formation (%)
CF-1/AuNPs	16.6	708	0.69 ± 0.06	0.80 ± 0.07
CF-2/AuNPs	10.6	453	0.39 ± 0.05	1.20 ± 0.12
CF-3/AuNPs	16.8	719	0.34 ± 0.05	0.90 ± 0.10
CF-4/AuNPs	8.2	350	0.74 ± 0.06	1.20 ± 0.12
CF-5/AuNPs	5.8	247	0.80 ± 0.07	1.00 ± 0.10

[a] Reaction conditions: -1.5 V vs Ag/AgCl in 0.1 M Na_2SO_4 containing 0.1 M xylose for 6 h duration at room temperature and pressure. The values reflected are the average from three measurements.

(1.2 %) and CF-5/AuNPs (1.0 %) toward xylose ECH were also comparable or higher than for the other CF/AuNPs catalyst. Xylose ECH was also carried out using only the CF support as catalyst at the same reaction conditions. However, negligible amounts of xylitol was formed which indicates that the catalytic activity of the CF/AuNPs catalysts is largely due to the AuNPs present.

From the results of the electrocatalytic hydrogenation of glucose and xylose, it is evident that chemical or thermal pretreatment of the CF support had a direct effect on the activity of the resulting CF/AuNPs catalysts. One factor that would influence this is the particle size distribution of AuNPs, resulting from the type of CF pretreatment carried out. Fig. 7 shows the ECSA-normalized activities of the CF/AuNPs catalysts towards glucose (Fig. 7a) and xylose (Fig. 7b) ECH as a function of the average Au particle size. For the glucose ECH, the sorbitol yield was observed to increase with increasing average Au particle size (Fig. 7a) up to 18.9 nm, which was measured for CF-4/AuNPs. CF-4/AuNPs also had the highest *FE* among the tested CF/AuNPs catalysts. The same trend was observed for the xylose ECH (Fig. 7b), with the highest xylitol yield obtained from the catalyst with the largest Au average particle size (CF-5/AuNPs - 20.6 nm). The *FE* however, was highest for CF-4/AuNPs and CF-2/AuNPs with slightly smaller average Au particle size of 18.9 and 19.9 nm, respectively. The sugar alcohol yields and *FE* were relatively lower for CF-1/AuNPs and CF-3/AuNPs with lower average Au particle sizes of 10.2 and 7.6 nm, respectively. CF-1/AuNPs and CF-3/AuNPs recorded the highest current densities in both glucose and xylose ECH. This means that CF-1/AuNPs and CF-3/AuNPs catalysts were more selective towards H_2 formation. This is consistent with earlier observations that smaller AuNPs favor H_2 evolution due to stronger binding of adsorbed hydrogen [45]. This was also evident in the linear sweep voltammograms recorded in the background electrolyte (Figure S4), where higher cathodic currents were observed for CF-1/AuNPs, CF-2/AuNPs, and CF-3/AuNPs with relatively higher fraction of smaller AuNPs than in the other catalysts.

3.2.3. *Reaction pathways for the ECH of glucose and xylose*

Aside from the physicochemical properties of the catalyst, the pH changes at the catalyst-solution interface also plays a significant role in the hydrogenation of both glucose and xylose. The formation of adsorbed hydrogen (Eq. (1)) and H_2 evolution (Eq. (3)) produce hydroxide ions, thereby increasing the interfacial pH in the vicinity of the catalyst surface. An increase in pH at the cathode surface is necessary to convert the cyclic forms of glucose and xylose into the linear (electroactive) forms [7,46], which are subsequently hydrogenated to sorbitol and xylitol, respectively (Scheme 1). To confirm this, ECH of glucose and xylose was carried out at pH 7 using phosphate buffer. After 6 hours of electrolysis, no sorbitol or xylitol product was observed, which indicates that glucose or xylose was not reactive at neutral pH. However, in an unbuffered solution, a continuous production of hydroxide ions during the constant-potential electrolyses results in an increase of pH in the bulk catholyte. This then results in the base-catalyzed isomerization of glucose into fructose (Scheme 1a), and xylose into xylulose (Scheme 1b). The formation of ketose and sugar alcohol products proceeds through an enediol intermediate formed from the reaction of base with the starting sugar. The reaction between the enediol intermediate with adsorbed hydrogen produces isomeric sugar alcohol products. HPLC analysis of reaction products show that mannitol, aside from sorbitol, was formed during glucose ECH. The concentration of the fructose by-product of glucose ECH on the different CF/AuNPs catalysts and the relative amounts of sorbitol and mannitol formed are illustrated in Figure S15a. In the same manner, xylulose was formed alongside xylitol and arabitol (Scheme 1b). The amounts of xylulose formed from the xylose ECH on the different CF/AuNPs catalysts and the relative amounts of xylitol and arabitol produced are shown in Fig S15b. As shown in Figure S15, the sorbitol/mannitol and xylitol/arabitol ratios vary among the different types of CF/AuNPs catalysts. The apparent selectivity of the CF/AuNPs to the formation of sugar alcohol products is currently investigated.

4. Conclusions

In this work, the electrocatalytic hydrogenation of glucose and xylose on activated carbon fiber-supported Au nanoparticles (CF/AuNPs) was studied. Depending on the pre-treatment of the CF support, different Au particle size distributions were obtained for the various CF/AuNPs catalysts prepared. This in turn gave rise to variations in catalytic activity and selectivity among the different types of CF/AuNPs catalysts. As observed, CF/AuNPs with smaller Au particle sizes were more active towards HER and showed less selectivity towards glucose and xylose ECH than CF/AuNPs with larger AuNPs. This indicates that the electrocatalytic activity and selectivity of Au towards hydrogenation of glucose and xylose is particle size-dependent. However, due to the relatively wide Au particle size distribution of the CF/AuNPs studied in this work, it is difficult to pinpoint an optimum ECH activity to a particular particle size range. Glucose and xylose ECH was also compared between a CF/AuNPs catalyst and a polycrystalline Au catalyst, and relatively higher ECH rates were observed for CF/AuNPs. The higher catalytic activity of CF/AuNPs is related to its higher surface area and more surface active sites available for sugar hydrogenation. Aside from the properties of the catalyst, careful pH control of the reaction solution is also essential for the selective ECH of glucose and xylose to sorbitol and xylitol, respectively. This is particularly important for

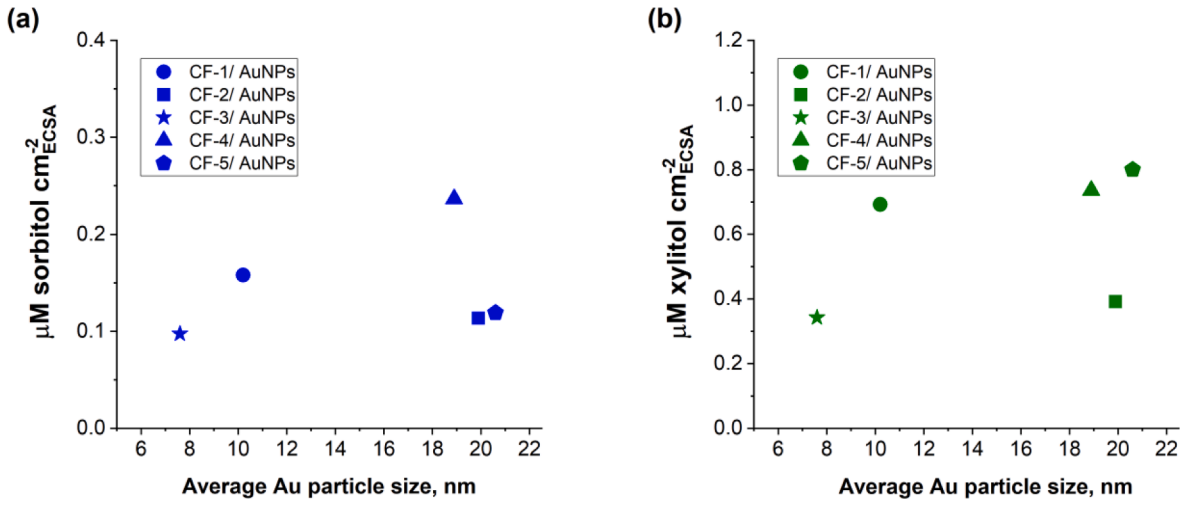

Fig. 7. The dependence of the activities towards glucose (a) and xylose (b) ECH on the average Au particle size of the CF/AuNPs catalyst.

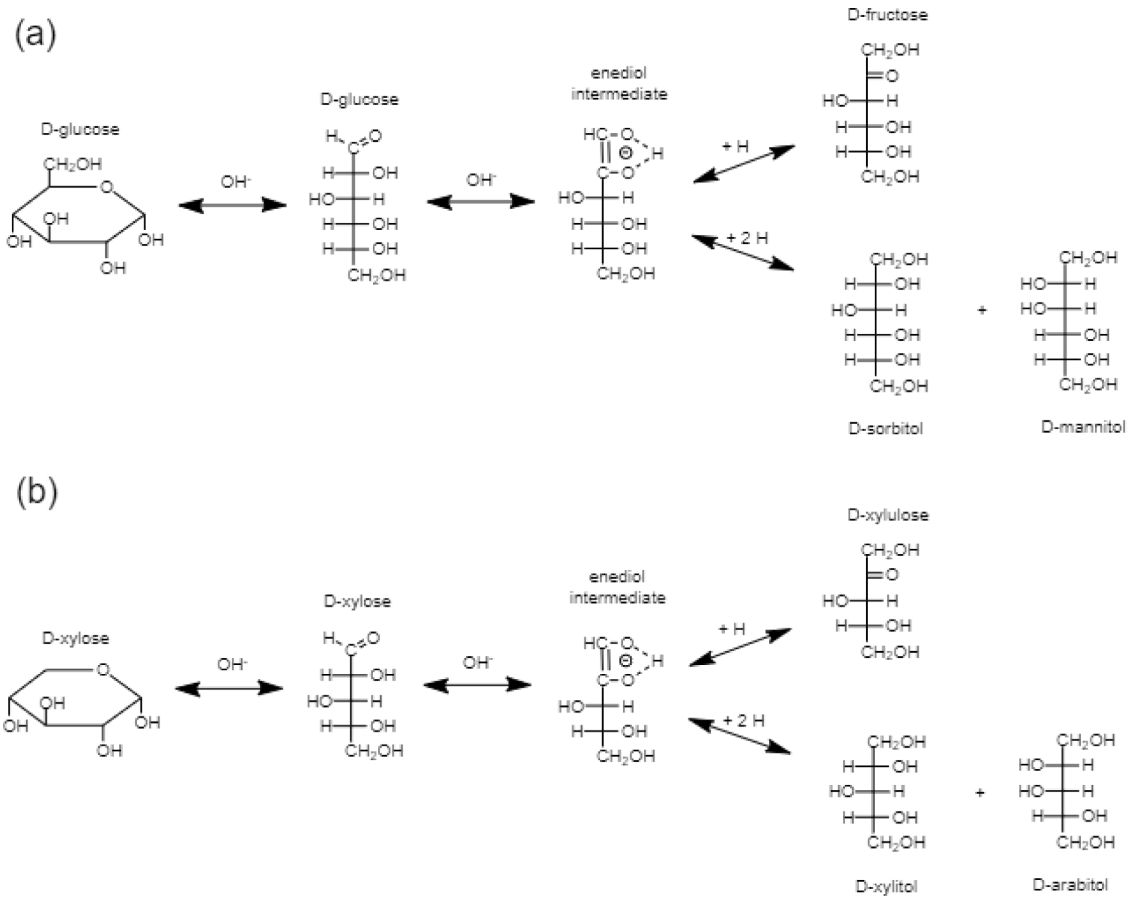

Scheme 1. Suggested reaction schemes for the hydrogenation of glucose (a) and xylose (b).

prolonged electrolyses in batch configuration, in which the high pH in the bulk brought about by HER would result in the base-catalyzed isomerization of the starting sugar.

CRediT authorship contribution statement

Jay Pee Oña: Investigation, Data curation, Writing – original draft. **Rose-Marie Latonen:** Methodology, Investigation, Writing – review & editing, Supervision. **Narendra Kumar:** Methodology, Investigation, Writing – review & editing. **Markus Peurla:** Investigation. **Ilari Angervo:** Investigation. **Henrik Grénman:** Conceptualization, Methodology, Writing – review & editing, Supervision, Data curation, Funding acquisition.

Declaration of Competing Interest

The authors declare that they have no known competing financial interests or personal relationships that could have appeared to influence the work reported in this paper.

Acknowledgments

This research is part of the FosToBioH2 (From fossil to biohydrogen in Finnish (bio)industry - utilizing electrocatalysis in Aqueous Phase Reforming of hemicelluloses) project at Åbo Akademi University, Finland. The authors gratefully acknowledge the Tiina and Antti Herlin Foundation (Finland) for their significant financial support. We also thank the Electron Microscopy Laboratory, Institute of Biomedicine, University of Turku, and Biocenter Finland for the TEM images and L. Silvander (Åbo Akademi University) for the SEM analysis.

Supplementary materials

Supplementary material associated with this article can be found, in the online version, at doi:10.1016/j.electacta.2022.140754.

References

[1] G.W. Huber, S. Iborra, A. Corma, Synthesis of transportation fuels from biomass: chemistry, catalysts, and engineering, Chem. Rev. 106 (2006), https://doi.org/10.1021/cr068360d.
[2] S.A. Akhade, N. Singh, O.Y. Gutierrez, J. Lopez-Ruiz, H. Wang, J.D. Holladay, Y. Liu, A. Karkamkar, R.S. Weber, A.B. Padmaperuma, M.S. Lee, G.A. Whyatt, M. Elliott, J.E. Holladay, J.L. Male, J.A. Lercher, R. Rousseau, V.A. Glezakou, Electrocatalytic hydrogenation of biomass-derived organics: a review, Chem. Rev. 120 (2020), https://doi.org/10.1021/acs.chemrev.0c00158.
[3] B. Chen, U. Dingerdissen, J.G.E. Krauter, H.G.J. Lansink Rotgerink, K. Möbus, D. J. Ostgard, P. Panster, T.H. Riermeier, S. Seebald, T. Tacke, H. Trauthwein, New developments in hydrogenation catalysis particularly in synthesis of fine and intermediate chemicals, Appl. Catal. A 280 (2005), https://doi.org/10.1016/j.apcata.2004.08.025.
[4] T.L. Levalley, A.R. Richard, M. Fan, The progress in water gas shift and steam reforming hydrogen production technologies - a review, Int. J. Hydrog. Energy 39 (2014), https://doi.org/10.1016/j.ijhydene.2014.08.041.
[5] F.W.S. Lucas, R.G. Grim, S.A. Tacey, C.A. Downes, J. Hasse, A.M. Roman, C. A. Farberow, J.A. Schaidle, A. Holewinski, Electrochemical routes for the valorization of biomass-derived feedstocks: from chemistry to application, ACS Energy Lett. 6 (2021), https://doi.org/10.1021/acsenergylett.0c02692.
[6] L. Du, Y. Shao, J. Sun, G. Yin, C. Du, Y. Wang, Electrocatalytic valorisation of biomass derived chemicals, Catal. Sci. Technol. 8 (2018), https://doi.org/10.1039/c8cy00533h.
[7] Y. Kwon, M.T.M. Koper, Electrocatalytic hydrogenation and deoxygenation of glucose on solid metal electrodes, ChemSusChem 6 (2013), https://doi.org/10.1002/cssc.201200722.
[8] P.N. Pintauro, J.R. Bontha, The role of supporting electrolyte during the electrocatalytic hydrogenation of aromatic compounds, J. Appl. Electrochem. 21 (1991), https://doi.org/10.1007/BF01402817.

[9] T. Yamada, T. Osa, T. Matsue, Hydrogenation of benzene ring by paired electrosynthesis with raney-nickel cathode, Chem. Lett. 16 (1987), https://doi.org/10.1246/cl.1987.1989.

[10] G. Belot, S. Desjardins, J. Lessard, Electrocatalytic hydrogenation of organic compounds on Devarda copper and Raney nickel electrodes in basic media, Tetrahedron Lett. 25 (1984), https://doi.org/10.1016/S0040-4039(01)91280-8.

[11] J. Lessard, G. Belot, Y. Couture, S. Desjardins, C. Roy, The use of hydrogen generated at the electrode surface for electrohydrogenation of organic compounds, Int. J. Hydrogen Energy 18 (1993), https://doi.org/10.1016/0360-3199(93)90122-Q.

[12] G. Horányi, A radiotracer study of the adsorption and electrocatalytic reduction of nicotinic acid at a platinized platinum electrode, J. Electroanal. Chem. (1990) 284, https://doi.org/10.1016/0022-0728(90)85052-7.

[13] K. Amouzegar, O. Savadogo, Electrocatalytic hydrogenation of phenol on dispersed Pt: Reaction mechanism and support effect, Electrochim. Acta 43 (1997), https://doi.org/10.1016/S0013-4686(97)00131-X.

[14] K. Amouzegar, O. Savadogo, Electrocatalytic hydrogenation of phenol on dispersed Pt: Effect of metal electrochemically active surface area and electrode material, J. Appl. Electrochem. (1997) 27, https://doi.org/10.1023/A:1018442527348.

[15] K. Amouzegar, O. Savadogo, Electrocatalytic hydrogenation of phenol on highly dispersed Pt electrodes, Electrochim. Acta 39 (1994), https://doi.org/10.1016/0013-4686(94)80101-0.

[16] U. Sanyal, J. Lopez-Ruiz, A.B. Padmaperuma, J. Holladay, O.Y. Gutiérrez, Electrocatalytic hydrogenation of oxygenated compounds in aqueous phase, Org. Process Res. Dev. 22 (2018), https://doi.org/10.1021/acs.oprd.8b00236.

[17] U. Sanyal, K. Koh, L.C. Meyer, A. Karkamkar, O.Y. Gutiérrez, Simultaneous electrocatalytic hydrogenation of aldehydes and phenol over carbon-supported metals, J. Appl. Electrochem. 51 (2021), https://doi.org/10.1007/s10800-020-01464-7.

[18] Y. Song, U. Sanyal, D. Pangotra, J.D. Holladay, D.M. Camaioni, O.Y. Gutiérrez, J. A. Lercher, Hydrogenation of benzaldehyde via electrocatalysis and thermal catalysis on carbon-supported metals, J. Catal. 359 (2018), https://doi.org/10.1016/j.jcat.2017.12.026.

[19] J.A. Lopez-Ruiz, E. Andrews, S.A. Akhade, M.S. Lee, K. Koh, U. Sanyal, S.F. Yuk, A. J. Karkamkar, M.A. Derewinski, J. Holladay, V.A. Glezakou, R. Rousseau, O. Y. Gutiérrez, J.D. Holladay, Understanding the role of metal and molecular structure on the electrocatalytic hydrogenation of oxygenated organic compounds, ACS Catal. 9 (2019), https://doi.org/10.1021/acscatal.9b02921.

[20] J.A. Lopez-Ruiz, U. Sanyal, J. Egbert, O.Y. Gutiérrez, J. Holladay, Kinetic investigation of the sustainable electrocatalytic hydrogenation of benzaldehyde on Pd/C: effect of electrolyte composition and half-cell potentials, ACS Sustain. Chem. Eng. 6 (2018), https://doi.org/10.1021/acssuschemeng.8b02637.

[21] T.S. Dalavoy, J.E. Jackson, G.M. Swain, D.J. Miller, J. Li, J. Lipkowski, Mild electrocatalytic hydrogenation of lactic acid to lactaldehyde and propylene glycol, J. Catal. (2007) 246, https://doi.org/10.1016/j.jcat.2006.11.009.

[22] B. Zhao, M. Chen, Q. Guo, Y. Fu, Electrocatalytic hydrogenation of furfural to furfuryl alcohol using platinum supported on activated carbon fibers, Electrochim. Acta 135 (2014), https://doi.org/10.1016/j.electacta.2014.04.164.

[23] K. Park, P.N. Pintauro, M.M. Baizer, K. Nobe, Flow reactor studies of the paired electro-oxidation and electroreduction of glucose, J. Electrochem. Soc. 132 (1985), https://doi.org/10.1149/1.2114229.

[24] J.C. Yu, M.M. Baizer, K. Nobe, Mathematical modeling of the paired electro-organic syntheses in packed bed flow reactors: II . Gluconate and sorbitol from glucose, J. Electrochem. Soc. 135 (1988), https://doi.org/10.1149/1.2096004.

[25] A. bin Kassim, C.L. Rice, A.T. Kuhn, Formation of sorbitol by cathodic reduction of glucose, J. Appl. Electrochem. 11 (1981), https://doi.org/10.1007/BF00610988.

[26] P.N. Pintauro, D.K. Johnson, K. Park, M.M. Baizer, K. Nobe, The paired electrochemical synthesis of sorbitol and gluconic acid in undivided flow cells. I, J. Appl. Electrochem. 14 (1984), https://doi.org/10.1007/BF00618739.

[27] S. Fei, J. Chen, S. Yao, G. Deng, L. Nie, Y. Kuang, Electroreduction of α-glucose on CNT/graphite electrode modified by Zn and Zn-Fe alloy, J. Solid State Electrochem. 9 (2005), https://doi.org/10.1007/s10008-004-0585-y.

[28] Y. Owobi-Andely, K. Fiaty, P. Laurent, C. Bardot, Use of electrocatalytic membrane reactor for synthesis of sorbitol, Catal. Today 56 (2000), https://doi.org/10.1016/S0920-5861(99)00274-6.

[29] Z. Liang, M.A. Villalba, G. Marcandalli, K. Ojha, A.J. Shih, M.T.M. Koper, Electrochemical reduction of the simplest monosaccharides: dihydroxyacetone and glyceraldehyde, ACS Catal. 10 (2020), https://doi.org/10.1021/acscatal.0c04131.

[30] P. Mäki-Arvela, B. Holmbom, T. Salmi, D.Y. Murzin, Recent progress in synthesis of fine and specialty chemicals from wood and other biomass by heterogeneous catalytic processes, Catal. Rev. Sci. Eng. (2007) 49, https://doi.org/10.1080/01614940701313127.

[31] M. Andérez Fernández, J. Rissanen, A. Pérez Nebreda, C. Xu, S. Willför, J. García Serna, T. Salmi, H. Grénman, Hemicelluloses from stone pine, holm oak, and Norway spruce with subcritical water extraction – comparative study with characterization and kinetics, J. Supercrit. Fluids 133 (2018), https://doi.org/10.1016/j.supflu.2017.07.001.

[32] F.M. Yedro, H. Grénman, J.v. Rissanen, T. Salmi, J. García-Serna, M.J. Cocero, Chemical composition and extraction kinetics of Holm oak (Quercus ilex) hemicelluloses using subcritical water, J. Supercrit. Fluids (2017) 129, https://doi.org/10.1016/j.supflu.2017.01.016.

[33] G. Gallina, Á. Cabeza, H. Grénman, P. Biasi, J. García-Serna, T. Salmi, Hemicellulose extraction by hot pressurized water pretreatment at 160 ^{o}C for 10 different woods: Yield and molecular weight, J. Supercrit. Fluids 133 (2018), https://doi.org/10.1016/j.supflu.2017.10.001.

[34] A.P. Nebreda, H. Grénman, P. Mäki-Arvela, K. Eränen, J. Hemming, S. Willför, D. Y. Murzin, T. Salmi, Acid hydrolysis of O-acetyl-galactoglucomannan in a continuous tube reactor: A new approach to sugar monomer production, Holzforschung (2016) 70, https://doi.org/10.1515/hf-2014-0314.

[35] X. Lu, P. Junghans, J. Wärnå, G. Hilpmann, R. Lange, H. Trajano, K. Eränen, L. Estel, S. Leveneur, H. Grénman, Hydrolysis of semi-industrial aqueous extracted xylan from birch (Betula pendula) employing commercial catalysts: kinetics and modelling, J. Chem. Technol. Biotechnol. (2022) 97, https://doi.org/10.1002/jctb.6918.

[36] X. Lu, P. Junghans, S. Weckesser, J. Wärnå, G. Hilpmann, R. Lange, H. Trajano, K. Eränen, L. Estel, S. Leveneur, H. Grénman, One flow through hydrolysis and hydrogenation of semi-industrial xylan from birch (betula pendula) in a continuous reactor—Kinetics and modelling, Chem. Eng. Process. - Process Intensif. (2021) 169, https://doi.org/10.1016/j.cep.2021.108614.

[37] P. Gallezot, P.J. Cerino, B. Blanc, G. Flèche, P. Fuertes, Glucose hydrogenation on promoted raney-nickel catalysts, J. Catal. 146 (1994), https://doi.org/10.1016/0021-9517(94)90012-4.

[38] T. Pepper, P.M. Olinger, Xylitol in sugar-free confections, Food Technol. 42 (1988).

[39] E. Behravesh, N. Kumar, Q. Balme, J. Roine, J. Salonen, A. Schukarev, J. P. Mikkola, M. Peurla, A. Aho, K. Eränen, D.Y. Murzin, T. Salmi, Synthesis and characterization of Au nano particles supported catalysts for partial oxidation of ethanol: Influence of solution pH, Au nanoparticle size, support structure and acidity, J. Catal. 353 (2017), https://doi.org/10.1016/j.jcat.2017.07.014.

[40] M. Thommes, K. Kaneko, A.v. Neimark, J.P. Olivier, F. Rodriguez-Reinoso, J. Rouquerol, K.S.W. Sing, Physisorption of gases, with special reference to the evaluation of surface area and pore size distribution (IUPAC Technical Report), Pure Appl. Chem. 87 (2015), https://doi.org/10.1515/pac-2014-1117.

[41] S. Trasa, A. Petrii, K. Niki, International Union of Pure and Applied Chemistry Real Surface Area Measurements in Electrochemistry, J. N. Agar (UK J. Koryta (Czechoslovakia Plieth (FRG. 321 (1992).

[42] P.A. Simonov, A.v. Romanenko, I.P. Prosvirin, G.N. Kryukova, A.L. Chuvilin, S. v. Bogdanov, E.M. Moroz, V.A. Likholobov, Electrochemical behaviour of quasi-graphitic carbons at formation of supported noble metal catalysts, Stud. Surf. Sci. Catal. (1998), https://doi.org/10.1016/S0167-2991(98)80164-X.

[43] L. Prati, G. Martra, New gold catalysts for liquid phase oxidation, Gold Bull. 32 (1999), https://doi.org/10.1007/BF03216617.

[44] L. Prati, M. Rossi, Gold on carbon as a new catalyst for selective liquid phase oxidation of diols, J. Catal. 176 (1998), https://doi.org/10.1006/jcat.1998.2078.

[45] W. Zhu, R. Michalsky, Ö. Metin, H. Lv, S. Guo, C.J. Wright, X. Sun, A.A. Peterson, S. Sun, Monodisperse Au nanoparticles for selective electrocatalytic reduction of CO2 to CO, J. Am. Chem. Soc. 135 (2013), https://doi.org/10.1021/ja409445p.

[46] W.W. Pigman, R.M. Goepp, Chemistry of the Carbohydrates, Academic Press, 1948.